Combined Supine and Prone Quantitative Myocardial Perfusion SPECT: Method Development and Clinical Validation in Patients with No Known Coronary Artery Disease

Hidetaka Nishina, MD[1]; Piotr J. Slomka, PhD[1,2]; Aiden Abidov, MD, PhD[1]; Shunichi Yoda, MD[1]; Cigdem Akincioglu, MD[1]; Xingping Kang, MD[1]; Ishac Cohen, PhD[1]; Sean W. Hayes, MD[1,2]; John D. Friedman, MD[1,2]; Guido Germano, PhD[1,2]; and Daniel S. Berman, MD[1,2]

[1]Departments of Imaging and Medicine and CSMC Burns & Allen Research Institute, Cedars-Sinai Medical Center, Los Angeles, California; and [2]Department of Medicine, David Geffen School of Medicine at UCLA, Los Angeles, California

Acquisition in the prone position has been demonstrated to improve the specificity of visually analyzed myocardial perfusion SPECT (MPS) for detecting coronary artery disease (CAD). However, the diagnostic value of prone imaging alone or combined acquisition has not been previously described using quantitative analysis. **Methods:** A total of 649 patients referred for MPS comprised the study population. Separate supine and prone normal limits were derived from 40 males and 40 females with a low likelihood (LLk) of CAD using a 3 average-deviation cutoff for all pixels on the polar map. These limits were applied to the test population of 369 consecutive patients (65% males; age, 65 ± 13 y; 49% exercise stress) without known CAD who had diagnostic coronary angiography within 3 mo of MPS. Total perfusion deficit (TPD), defined as a product of defect extent and severity scores, was obtained for supine (S-TPD), prone (P-TPD), and combined supine–prone datasets (C-TPD). The angiographic group was randomly divided into 2 groups for deriving and validating optimal diagnostic cutoffs. Normalcy rates were validated in 2 additional groups of consecutive LLk patients: unselected patients (n = 100) and patients with body mass index >30 (n = 100). **Results:** C-TPD had a larger area under the receiver-operating-characteristic (ROC) curve than S-TPD or P-TPD for identification of stenosis ≥70% (0.86, 0.88, and 0.90 for S-TPD, P-TPD, and C-TPD, respectively; $P < 0.05$). In the validation group, sensitivity for P-TPD was lower than for S- or C-TPD ($P < 0.05$). C-TPD yielded higher specificity than S-TPD and a trend toward higher specificity than P-TPD (65%, 83%, and 86% for S-, P-, and C-TPD, respectively, $P < 0.001$; vs. S-TPD and $P = 0.06$ vs. P-TPD). Normalcy rates for C-TPD were higher than for S-TPD in obese LLk patients (78% vs. 95%, $P < 0.001$). **Conclusion:** Combined supine–prone quantification significantly improves the area under the ROC curve and specificity of MPS in the identification of obstructive CAD compared with quantification of supine MPS alone.

Key Words: myocardial perfusion SPECT; quantification; prone imaging; normal limits

J Nucl Med 2006; 47:51–58

Myocardial perfusion SPECT (MPS) has traditionally been performed with patients in the supine position. These images, however, are often associated with diaphragmatic attenuation of the inferior wall (*1,2*) and breast attenuation of the anterior wall in females (*3*), causing false-positive inferior and anterior wall defects that reduce test specificity. Segall et al., in 1988, initially described prone imaging of MPS (*4*). In 1989, Esquerre et al. (*5*) and Segall et al. (*6*) demonstrated that, for ^{201}Tl MPS, imaging patients in the prone position improved the specificity in evaluating inferior wall abnormalities by minimizing diaphragmatic attenuation. A subsequent study from our group reported overall sensitivity and specificity of 80% and 93% of prone MPS for the diagnosis of coronary artery disease (CAD) (*7*). Prone MPS has been reported to reduce the apparent myocardial counts of the anterior, anteroseptal, and lateral walls and sometimes cause false-positive defects in those regions. In our laboratory, for the last 10 y, we have been routinely performing combined supine and prone acquisitions for poststress images if patients can tolerate prone imaging.

Recently, a study from our group has shown that patients with inferior wall defects on supine MPS that are not present on prone MPS have a low risk of subsequent cardiac events, thus, prone MPS yields additional prognostic information as compared with supine MPS (*8*).

To date, the added diagnostic value of combining supine and prone imaging has not been reported quantitatively. Various approaches for the quantitative analysis of supine MPS images with ^{201}Tl as well as ^{99m}Tc-labeled myocardial

Received Jul. 5, 2005; revision accepted Sep. 27, 2005.

For correspondence or reprints contact: Daniel S. Berman, MD, Cedars-Sinai Medical Center, Room A1258, 8700 Beverly Blvd., Los Angeles, CA 90048.

E-mail: bermand@cshs.org

perfusion tracers have been developed and validated (*9–11*). Recently, we have developed and validated a quantification scheme in which normal limits are derived from patients with a low likelihood (LLk) of CAD without optimization of regional thresholds by expert visual scoring (*12*). This simplified approach of establishing normal limits has enabled us to derive additional normal limits, such as prone-acquisition normal limits, using scans of patients with a LLk of CAD. In this study, we develop and validate a new integrated supine–prone quantification scheme using both supine- and prone-specific normal limits and apply this approach to compare objectively the diagnostic accuracy of this combined supine–prone quantitation to supine alone quantification for detection of CAD.

MATERIALS AND METHODS

Total Population

The total study population consisted of 649 patients who underwent exercise or adenosine stress ^{99m}Tc-sestamibi MPS performed in both supine and prone position. These were consecutive patients who either had cardiac catheterization <3 mo after rest ^{201}Tl/^{99m}Tc-sestamibi gated dual-isotope MPS or who had a LLk of CAD (<5%) based on age, sex, symptoms, coronary risk factors, and results of rest and stress electrocardiography (*13*) at the time of MPS. Patients with excessive motion on projection images or with areas of excessive extracardiac uptake adjacent to the myocardium on reconstructed images were excluded ($n = 16$).

Normal Database Population: Group 1. Sex-specific normal limits for both supine and prone acquisitions were derived from a group of 80 patients (40 females, 40 males) with a LLk of CAD (Table 1). No patients in this group had diabetes mellitus, angina or shortness of breath, abnormal resting electrocardiogram (ECG), or abnormal stress ECG response. In this group only, an additional criterion for inclusion was normal rest and poststress MPS images by visual assessment. For visual interpretation of poststress MPS, both supine and prone images were assessed simultaneously and such combined supine–prone interpretation was required to be normal.

Normalcy Population: Group 2. To obtain normalcy rates, 2 additional groups of patients with a LLk of CAD were analyzed: 100 consecutive patients (group 2A), and another 100 consecutive obese patients, having a body mass index of >30 (group 2B), (Table 1). In group 2A, patients were included regardless of their body size and there was no overlap in patients between group 2A and group 2B.

Angiographic Validation Population: Group 3. This group consisted of 369 consecutive patients (241 males, 128 females) who had coronary angiography within 3 mo of MPS (Table 2). Exclusion criteria were as follows: (a) prior myocardial infarction or coronary revascularization; (b) nonischemic cardiomyopathy or valvular heart disease; and (c) change in symptoms between MPS and coronary angiography.

Acquisition and Reconstruction Protocols

MPS acquisitions were performed with a noncircular 180° orbit with 64 projections at 25 s/projection for supine ^{99m}Tc acquisition, followed immediately by 15 s/projection for prone ^{99m}Tc acquisition. Rest ^{201}Tl acquisition was performed at 35 s/projection (*14*) in supine position only. MPS used either Philips (Adac Forte or Vertex) or Siemens (E-Cam) cameras. High-resolution collimators were used. No attenuation or scatter correction was applied. After iterative reconstruction (12 iterations) with Butterworth prefiltering (cutoff, 0.66 cycle/pixel for supine ^{99m}Tc, 0.55 cycle/pixel for prone ^{99m}Tc; order 5), short-axis images were automatically generated (*15*).

Exercise MPS Protocol. Patients performed a symptom-limited exercise treadmill test with the standard Bruce protocol. At near-maximal exercise, ^{99m}Tc-sestamibi (925–1,480 MBq based on patient weight) was injected intravenously. Treadmill exercise was continued at maximal workload for 1 min and at one stage lower for 2 additional minutes when possible. ^{99m}Tc-Sestamibi MPS acquisition was started 15–30 min after radiopharmaceutical injection.

Adenosine MPS Protocol. Adenosine MPS was performed as previously described (*16*). Adenosine was infused at 140 μg/kg/min for 5 min. At the end of the second minute, ^{99m}Tc-sestamibi (925–1,480 MBq [25–40 mCi]) was injected and MPS acquisition was started approximately 60 min later. Whenever possible, during adenosine infusion, patients performed a low-level treadmill exercise, walking at 0% grade at 1–1.7 mph (*17*). With the latter protocol, imaging began 15–60 min after adenosine stress.

TABLE 1
Characteristics of Patients with Low Likelihood of CAD

Parameter	Group 1: normal limits ($n = 80$)	Group 2A ($n = 100$)	Group 2B ($n = 100$)
Age (y)	56 ± 14	48 ± 9*	47 ± 8*
Sex (female)	40 (50%)	63 (63%)	67 (67%)
Body mass index	27 ± 5	26 ± 5	38 ± 9†
Hypertension	39 (49%)	29 (29%)	51 (51%)‡
Hypercholesterolemia	44 (55%)	37 (37%)	43 (43%)
Smoking	2 (3%)	6 (6%)	2 (2%)
Exercise stress	57 (71%)	53 (53%)	51 (51%)*

*$P < 0.05$ vs. group 1.
†$P < 0.001$ vs. group 1 or group 2A.
‡$P < 0.01$ vs. group 2A.

TABLE 2
Characteristics of Patients with Angiography

Parameter	Value
Age (y)	65 ± 13
Sex (female)	128 (35%)
Body mass index	28 ± 5
Hypertension	241 (65%)
Diabetes	89 (24%)
Hypercholesterolemia	203 (55%)
Symptoms	
Asymptomatic	69 (19%)
Nonanginal chest pain	34 (9%)
Atypical angina	159 (43%)
Typical angina	72 (20%)
Shortness of breath	55 (15%)
Exercise test	185 (49%)

Perfusion Quantification

Supine and prone images were quantified separately using their respective supine and prone normal limits and previously developed simplified approach (*12*). Briefly, an ellipsoidal model and contours derived by the QGS algorithm (*18*) were used to extract polar map samples. Count normalization was implemented using the iterative scheme, similar to that previously applied for stress–rest image normalization (*19*). An optimal normalization factor was established by an iterative search for the minimal absolute count difference between the counts in the normal part of the myocardium and the corresponding count distribution in the normal database. This scheme avoided normalization based on an arbitrary selection of pixels (maximum or percentile maximum). Subsequently, an abnormality threshold of 3.0 average (mean absolute) deviations was applied, which is approximately equivalent to 2.5 SD, to estimate the extent of hypoperfusion. This value is similar to the threshold used in other MPS quantification methods (*20*). The perfusion defect extent was calculated as the percentage of the total surface area of the left ventricle for which test data were below the abnormality threshold. For comparing the supine and prone polar maps, a 17-segment model was used (*21*).

Calculation of Total Perfusion Deficit (TPD). This measure was designed to combine defect severity and extent in one parameter, based on clinical data indicating that the combination of defect extent and severity adds to prognostic assessment (*22*). A continuous severity score was assigned to each abnormal polar-map pixel. The range of abnormal scores was between 2.0 and 4.0 and was assigned by linear mapping based on the degree the perfusion value fell below the normal limit. A score of 4.0 was assigned to all pixels >70% below the normal limit; this threshold was derived from subjective criteria used for a score of 4 in visual reading. A normal score of 0.0 was applied for pixels below minimum abnormal score. Subsequently, TPD was defined as follows (*1*):

$$TPD = 100\% \cdot \sum_{a=0}^{a<A} \sum_{p=0}^{p<P} score(a,p)/(4 \cdot A \cdot P),$$

where a and p were the radial coordinates of the polar map, A and P were the maximum numbers of samples in each dimension, and score(a,p) was the pixel score at the polar map location (a, p). The theoretic maximum value for TPD was 100% for a case with no visible uptake (<70% below normal) in the entire left ventricular myocardium. In this study, only stress short-axis images were used in image analysis.

Combined Supine–Prone Quantification. In addition to deriving separate TPD measures for supine (S-TPD) and prone (P-TPD) MPS, we developed a novel quantification approach obtaining combined TPD (C-TPD) parameter, based on the findings of abnormality on both supine and prone images. C-TPD is calculated by limiting the TPD computation from the supine polar map to pixels, which have been quantified as abnormal on prone images. The same average deviation threshold (3.0) is used for supine and prone images (as in the analysis of separate images). Additionally, 2 empiric rules have been built into the quantification process. For anterior or apical supine defects in males, concomitant prone polar map abnormalities are not required as, in our experience, true defects in this location sometimes are not detected on prone quantification. This is due to the relatively broader normal limits caused by variable count attenuation in this region on male prone SPECT. Similarly, abnormal pixels in the inferior wall on prone polar maps but not on supine polar maps were considered abnormal in males because of wider normal limit variation in this region on supine images. The C-TPD parameter was expressed in the same units (percentage of the myocardium) as in the separate supine and prone TPD measures.

Coronary Angiography

Coronary angiography was performed with the standard Judkins approach, and all coronary angiograms were interpreted visually by experienced physicians. No patients had myocardial infarction or revascularization in the interval between MPS and coronary angiography. A stenosis of ≥70% luminal diameter narrowing was considered significant. Coronary angiographic findings are presented in Table 3.

Statistical Analysis

All continuous variables are expressed as mean ± 1 SD. Paired t tests were used to compare differences in paired continuous data and McNemar tests were used to compare differences in paired discrete data. For unpaired continuous data, 1-way ANOVA was used with the Bonferroni correction for multiple comparisons. All statistical tests were 2-tailed, and a value of $P < 0.05$ was considered significant. The receiver-operating-characteristic (ROC) curve analysis was performed to evaluate the ability of the quantification to predict ≥70% stenoses of coronary arteries. ROC curves were created using a step of 0.1%, for the TPD values. The differences between ROC curve areas (area ± SE) were compared using version 1.71 of the Analyze-It statistical package from Analyze-it Software Ltd. and the Hanley and McNeil comparison method for ROC curves, which requires that all tests be performed on the same subjects (*23*). The optimal sensitivity and specificity were defined as those yielding the minimal value for $(1 - \text{sensitivity})^2 + 0.95 \times (1 - \text{specificity})^2$ (*24*). For the overall detection of CAD, those operating points with higher sensitivity than specificity were considered in the search for the optimal point. To provide unbiased definition of sensitivity and specificity, we randomly divided the angiographic population (group 3) into pilot group and validation group and determined the optimal threshold for abnormality from ROC curves derived in the pilot group ($n = 163$). Subsequently, this threshold was used to evaluate sensitivity and specificity in the validation group ($n = 206$).

RESULTS

In Figure 1A, the average count distributions derived from 40 males and females with LLk of CAD (group 1) are

TABLE 3
Angiographic Characteristics

Parameter	No. of patients
Normal	116 (31%)
Single-vessel disease	133 (36%)
Double-vessel disease	71 (19%)
Triple-vessel disease	49 (13%)
LAD	150 (41%)
LCX	121 (33%)
RCA	141 (38%)

LAD = left anterior descending artery; LCX = left circumflex artery; RCA = right coronary artery.

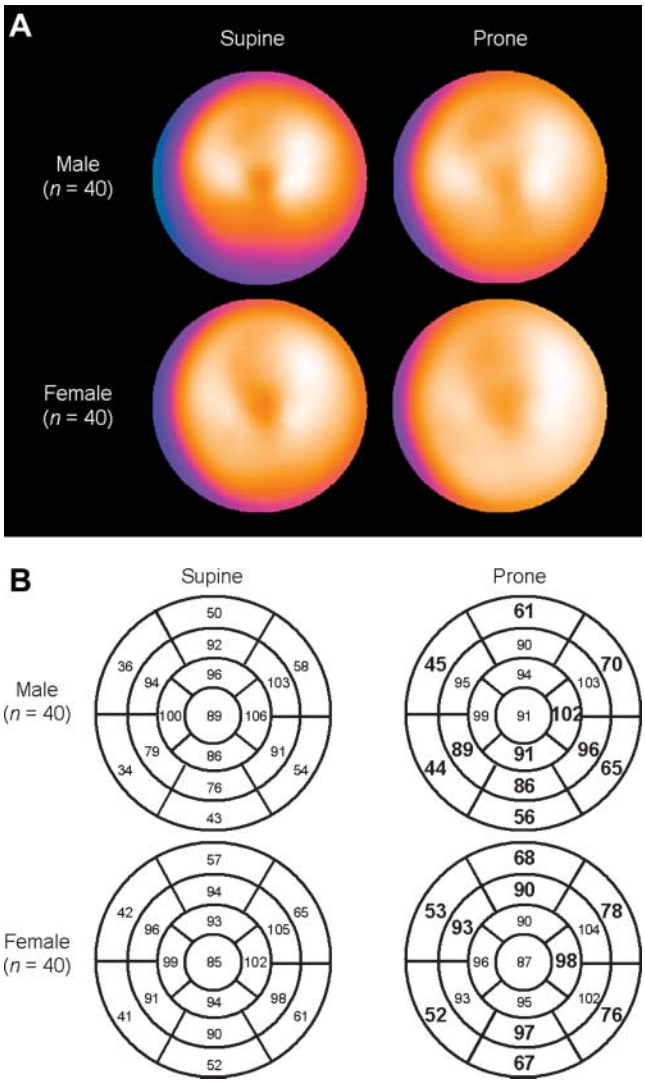

FIGURE 1. (A) Comparison of sex-specific mean myocardial perfusion distributions derived from LLk males ($n = 40$) and females ($n = 40$). (Top) Stress polar maps in males: supine (left) and prone (right). (Bottom) Corresponding female polar maps. (B) Segmental comparison of sex-dependent supine (left) and prone (right) mean normal perfusion distribution for males (top) and females (bottom). Bold and larger fonts denote significant difference between supine and prone images ($P < 0.05$).

presented using polar map display. In Figure 1B, count distributions are shown using a 17-segment model. The average myocardial uptake differed significantly between supine and prone in 11 of 17 segments in males and in 10 of 17 segments in females ($P < 0.05$). The segmental differences between supine and prone images were noted predominantly in the inferior distribution in males and in the anterior distribution in females (Fig. 1B).

Examples of combined supine–prone images are shown in Figures 2A–2C. Figure 2A illustrates a patient with normal coronary angiography who demonstrated an apparent inferior wall defect on supine images that is not detected by prone quantification or combined quantification. Figure 2B shows a patient with right coronary artery disease who showed an inferior wall defect on both supine and prone imaging that was detected by supine, prone, and combined quantification. Figure 2C shows a patient with a mid-to-distal inferior wall defect on supine images and quantification and an anteroseptal defect on prone images and quantification, with no significant defect detected by combined quantification.

The ROC curves for the detection of CAD by TPD measures derived from supine, prone, and combined supine–prone datasets are shown in Figure 3. The areas under the ROC curves for S-TPD, P-TPD, and C-TPD were 0.86 ± 0.02, 0.88 ± 0.02, and 0.90 ± 0.02, respectively. The area under the ROC curve for C-TPD was significantly higher than that for S-TPD ($P < 0.005$) or P-TPD ($P < 0.05$). There was no significant difference in the area under the ROC curves derived for S-TPD and P-TPD.

The optimal cutoff points were determined to be >5.5% of the maximal possible total perfusion deficit for S-TPD and P-TPD and >3.0% for C-TPD from the pilot group ($n = 163$). As shown in Figure 4, when these cutoffs were applied to the validation group, P-TPD had significantly lower sensitivity compared with S-TPD or C-TPD (85%, 77%, and 85% for S-TPD, P-TPD, and C-TPD; $P < 0.05$). On the other hand, P-TPD tended to have higher specificity than S-TPD (65% and 83% for S-TPD and P-TPD, respectively; $P = 0.06$), and C-TPD yielded significantly higher specificity than S-TPD (86%; $P < 0.01$). The accuracy was significantly higher for C-TPD (86%) than those for S-TPD (79%) or P-TPD (79%) ($P < 0.05$). Normalcy rates between 2 groups of patients with LLk of CAD are shown in Figure 5. There were no statistically significant differences in normalcy rates in the general LLk group (group 2A). C-TPD, however, yielded a significantly higher normalcy rate when compared with S-TPD in obese LLk patients (group 2B: 78%, 83%, and 95% for S-TPD, P-TPD, and C-TPD, respectively; $P < 0.001$ vs. S-TPD).

DISCUSSION

In this study we developed and validated a new approach for quantification of myocardial perfusion SPECT that integrates quantitative measures derived from datasets acquired in both supine and prone position. Separate sex-specific normal limits for both supine and prone MPS were derived from 40 males and females with a LLk of CAD. Thresholds for abnormality were prospectively developed in a pilot group and validated in a prospective group of MPS patients who also underwent coronary angiography within 3 mo. Normalcy rates in patient groups with a LLk of CAD were also evaluated. Our approach considers abnormality to be significant only when detected on both supine and prone images except for anterior, apical, and inferior wall for males. For anterior or apical supine defects in males, concomitant prone polar map abnormalities are not required. Similarly, abnormal pixels in the inferior wall on prone polar maps but not on supine polar maps were

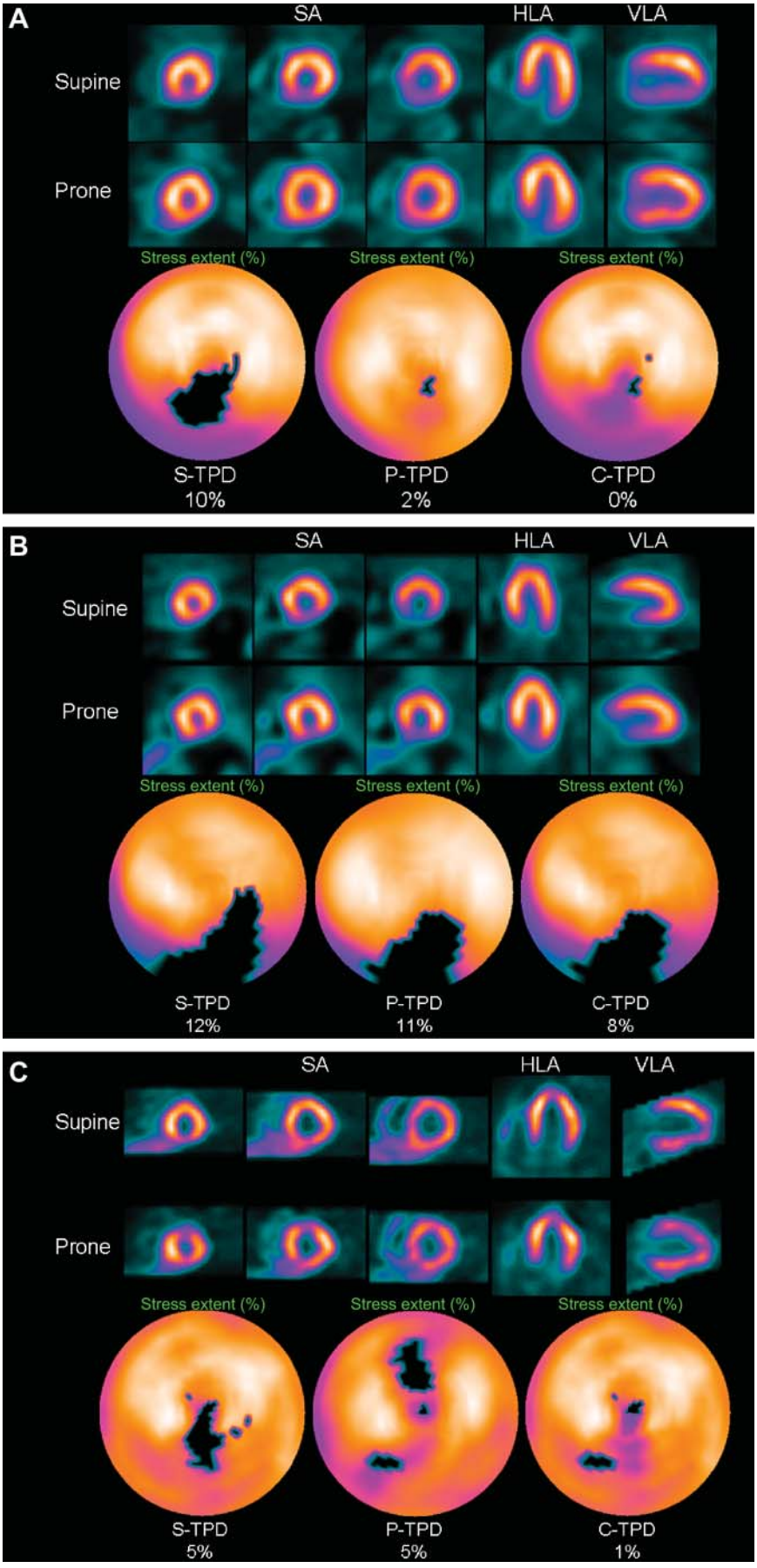

FIGURE 2. (A) Example of supine diaphragmatic attenuation artifact on MPS normalizing on prone MPS in 60-y-old male with history of diabetes, hypertension, hypercholesterolemia, and family history of premature CAD who achieved a heart rate of 148 (89% of maximum predicted heart rate). His body mass index was 34 and the ECG response to exercise stress was ischemic for ST-segment depression. Subsequent coronary angiogram showed no significant stenosis. Images displayed in 3 short axis (SA), horizontal long axis (HLA), and vertical long axis (VLA) reveal apparent perfusion abnormality in inferior wall in supine images (top row); however, prone images show uniform tracer distribution (middle row). Quantitative results shown as black-out maps (bottom row) show 10% S-TPD, 2% P-TPD, and 0% C-TPD, consistent with absence of CAD. (B) Example of true inferior wall defect on supine and prone images. MPS images from 75-y-old male with atypical chest pain and known hypercholesterolemia are presented. ECG response to exercise was ischemic for ST-segment depression and subsequent coronary angiogram revealed occlusion of proximal right coronary artery. Both supine (top row) and prone (middle row) images show apparent inferior wall perfusion abnormality and S-TPD, P-TPD, and C-TPD are 12%, 11%, and 8%, respectively, and defects are visualized on black-out maps (bottom row). (C) Example of anterior prone MPS artifact and inferior supine MPS artifact in 53-y-old asymptomatic male with abnormal resting ECG. Poststress supine images show reduced uptake of radiotracer in inferior wall (top row). Prone images, however, reveal anterior wall defect (middle row). Black-out maps are shown (bottom row) and quantification results were 5% for S-TPD and 5% for P-TPD. When supine and prone images are combined, only a small defect is visualized on black-out map, with C-TPD of 1% (bottom row)

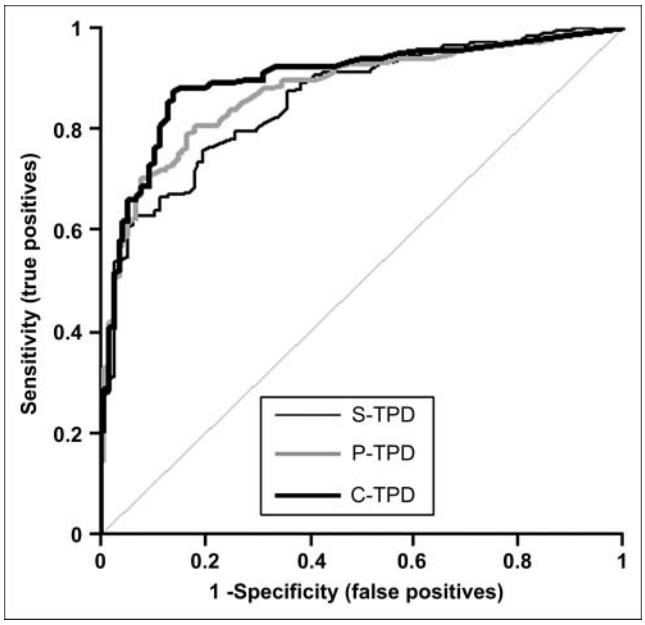

FIGURE 3. ROC curves for detection of CAD by measures of S-TPD, P-TPD, and C-TPD in angiographic population (n = 369).

considered abnormal in males in this study. Prospective comparison between supine, prone, and combined quantification for detecting angiographically significant CAD demonstrated that C-TPD yielded significant gains in the specificity over supine-only quantification without compromising sensitivity. In addition, it improved the normalcy rate in obese patients with a LLk of CAD.

A common problem with MPS is the artifactual reduction in apparent radiotracer uptake due to soft-tissue attenuation, resulting in reduced accuracy of interpretation. Most commonly, photon attenuation results in reduced specificity for detecting CAD; however, attenuation can

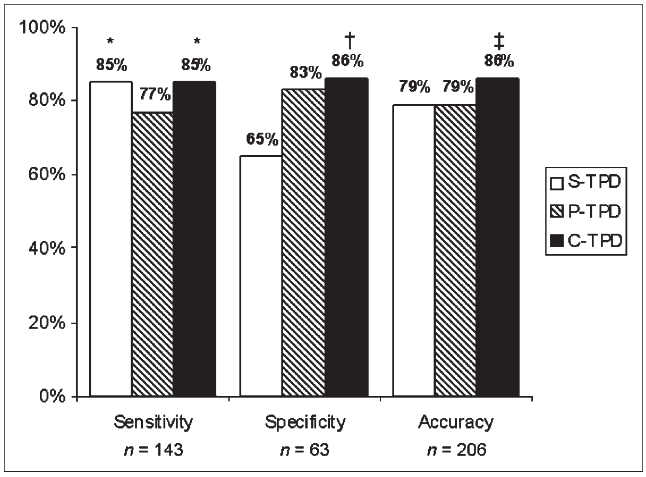

FIGURE 4. Optimal sensitivities, specificities, and accuracies for detection of CAD by S-TPD, P-TPD, and C-TPD in validation group (n = 206). *$P < 0.05$ vs. S-TPD or P-TPD; †$P < 0.001$ vs. S-TPD; ‡$P < 0.01$ vs. S-TPD or P-TPD.

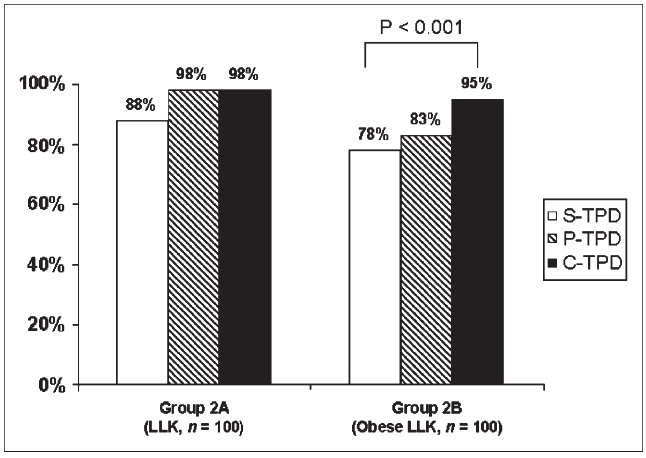

FIGURE 5. Normalcy rates in 2 groups of patients with LLk of CAD.

also affect sensitivity by increasing the range of normal limits. Various methods have been investigated to solve this problem. Inspecting planar projection images can help in identifying photon attenuation in the inferior wall due to the left hemidiaphragm or in the anterior wall in females with large breasts (*25*). However, relying exclusively on planar images for this purpose is likely to reduce sensitivity for the detection of true abnormalities. Cinematic display of wall motion and wall thickening from gated MPS has been shown to improve diagnostic certainty and effectively differentiate artifacts from true perfusion defects in equivocal fixed defects (*26–28*). Choi et al. reported improvement of specificity from 86% to 92% and sensitivity from 72% to 80% when gated images were reviewed along with tomographic perfusion images in patients with equivocal fixed defects (*26*). Smanio et al. demonstrated that adding gated cine images to rest–stress perfusion images alone resulted in reducing borderline interpretations (*28*). However, such addition of gated information to perfusion interpretation does not provide an optimal solution because, by considering fixed defects to be significant only when associated with abnormal contraction, true myocardial perfusion defects due to subendocardial infarction without associated contraction abnormality might be falsely attributed to soft-tissue attenuation (*29*). In addition, gated MPS is not useful in distinguishing shifting attenuation artifacts from true reversible perfusion defects (*25*). Nonuniform attenuation correction has also been shown to improve the specificity and normalcy rate of MPS (*30,31*). This approach, however, requires specialized hardware and software, and in some implementations may overcorrect the inferior wall, leading to lower sensitivity for detection of a true perfusion defect (*32*). By comparison, prone imaging requires additional acquisition of 10–12 min but can be performed on virtually any SPECT camera without the need for specialized hardware or software.

The prone position has been shown to reduce diaphragmatic attenuation and patient motion on MPS (*4,5,7*). The

reduced attenuation is considered to be due to a downward displacement of the diaphragm relative to the myocardium in the prone position (*6*), and the reduced patient motion is considered to be due to the close contact of the anterior portion of the chest to the imaging table (*7*). The prone acquisition, however, has also been reported to produce artifactual anteroseptal defects, thought to be due to the closer position of the heart to the bony structures of the anterior chest wall (*7*). We have previously documented that in patients who have inferior wall perfusion defects and normal prone images, the prognosis is excellent and equal to that observed in a cohort of patients with normal MPS using supine imaging alone (*8*). Since 1995, we have performed combined supine and prone imaging as a routine in all patients and have found that approximately 90% of patients are able to tolerate the prone position for the period required for adequate count statistics. Of note, the prone images are used for perfusion only and not for the assessment of function and, therefore, they are acquired without gating and for a 40% shorter time than the supine images.

We have not previously published our results for detecting CAD and normalcy rates with combined supine and prone MPS, because we previously did not have an objective method of comparing supine with combined supine and prone imaging in the same patients. We reasoned that if the observers in our laboratory were asked to read the supine only vs. the supine and prone images, an unconscious bias toward the combined imaging might exaggerate differences in the approaches. In this study we introduced and validated a novel concept of combined MPS quantification based on polar maps of the same patient obtained in both supine and prone positions. This computer method allowed us to assess objectively the differences between supine, prone, and combined MPS. The C-TPD method mimics the visual analysis process when prone and supine images are compared for the presence of defects and artifacts. In our experience true perfusion defects are often less visually apparent on prone than on supine MPS. Thus, we developed separate, sex-specific normal limits for the quantification of supine and prone images. In a recent publication our group has shown the superiority of such a simplified approach for standard supine imaging (non-combined) over the former technique where the regional SD were hand-tuned by matching with visual scores (*12*). In this article we compare this improved simplified approach with the new combined method.

This study has several limitations. We limited the analysis to the stress images only, whereas in clinical practice all data are interpreted based on stress–rest images when stress is abnormal. However, the rest images were acquired only in supine position and combined quantification applies only to stress images. We excluded studies of patients with prior myocardial infarction or revascularization because the presence of a severe perfusion defect associated with a myocardial infarct might artificially elevate the sensitivity for detection of CAD in a population where the question of disease detection is not relevant. Therefore, the current study does not assess the accuracy of C-TPD in patients with prior myocardial infarction. We also excluded studies with poor technical quality, such as cases with excessive patient motion or with significant extracardiac uptake adjacent to the myocardium, which might have resulted in a higher false-positive rate.

CONCLUSION

Quantification of combined supine and prone myocardial perfusion SPECT has allowed an objective demonstration of improved specificity for CAD and normalcy rates with the combined acquisition as compared with supine MPS. Although the technique does lengthen the time of poststress imaging, combined supine and prone MPS provides a practical means of reducing the false-positive rate associated with supine MPS.

ACKNOWLEDGMENTS

This work was presented in part at the American College of Cardiology 54th Annual Scientific Session, Orlando, FL, March 6–9, 2005. This work was supported in part by grants from Bristol-Myers Squibb Medical Imaging, Inc. (Billerica, MA) and Astellas (Deerfield, IL). Guido Germano, Piotr J. Slomka, and Daniel S. Berman participate in royalties to Cedars-Sinai Medical Center for licensure of software used.

REFERENCES

1. Strauss HW, Boucher CA. Myocardial perfusion studies: lessons from a decade of clinical use. *Radiology.* 1986;160:577–584.
2. DePuey EG III. How to detect and avoid myocardial perfusion SPECT artifacts. *J Nucl Med.* 1994;35:699–702.
3. Cohen M, Touzery C, Cottin Y, et al. Quantitative myocardial thallium single-photon emission computed tomography in normal women: demonstration of age-related differences. *Eur J Nucl Med.* 1996;23:25–30.
4. Segall GM, Davis MJ, Goris ML. Improved specificity of prone versus supine thallium SPECT imaging. *Clin Nucl Med.* 1988;13:915–916.
5. Esquerre JP, Coca FJ, Martinez SJ, et al. Prone decubitus: a solution to inferior wall attenuation in thallium-201 myocardial tomography. *J Nucl Med.* 1989;30: 398–401.
6. Segall GM, Davis MJ. Prone versus supine thallium myocardial SPECT: a method to decrease artifactual inferior wall defects. *J Nucl Med.* 1989;30: 548–555.
7. Kiat H, Van Train KF, Friedman JD, et al. Quantitative stress-redistribution thallium-201 SPECT using prone imaging: methodologic development and validation. *J Nucl Med.* 1992;33:1509–1515.
8. Hayes SW, De Lorenzo A, Hachamovitch R, et al. Prognostic implications of combined prone and supine acquisitions in patients with equivocal or abnormal supine myocardial perfusion SPECT. *J Nucl Med.* 2003;44:1633–1640.
9. Germano G, Kavanagh P, Waechter P, et al. A new algorithm for the quantitation of myocardial perfusion SPECT. I. Technical principles and reproducibility. *J Nucl Med.* 2000;41:712–719.
10. Van Train KF, Garcia EV, Maddahi J, et al. Multicenter trial validation for quantitative analysis of same-day rest-stress technetium-99m-sestamibi myocardial tomograms. *J Nucl Med.* 1994;35:609–618.
11. Ficaro E, Kritzman J, Corbett J. Development and clinical validation of normal Tc-99m sestamibi database: comparison of 3D-MSPECT to CEqual [abstract]. *J Nucl Med.* 1999;40(suppl):125P.
12. Slomka PJ, Nishina H, Berman DS, et al. Automated quantification of myocardial perfusion SPECT using simplified normal limits. *J Nucl Cardiol.* 2005;12:66–77.

13. Diamond GA, Staniloff HM, Forrester JS, et al. Computer-assisted diagnosis in the noninvasive evaluation of patients with suspected coronary artery disease. *J Am Coll Cardiol.* 1983;1:444–455.
14. Berman DS, Kiat H, Friedman JD, et al. Separate acquisition rest thallium-201/stress technetium-99m sestamibi dual-isotope myocardial perfusion single-photon emission computed tomography: a clinical validation study. *J Am Coll Cardiol.* 1993;22:1455–1464.
15. Germano G, Kavanagh PB, Su HT, et al. Automatic reorientation of three-dimensional, transaxial myocardial perfusion SPECT images. *J Nucl Med.* 1995;36:1107–1114.
16. Amanullah AM, Kiat H, Friedman JD, et al. Adenosine technetium-99m sestamibi myocardial perfusion SPECT in women: diagnostic efficacy in detection of coronary artery disease. *J Am Coll Cardiol.* 1996;27:803–809.
17. Berman DS, Kang X, Hayes SW, et al. Adenosine myocardial perfusion single-photon emission computed tomography in women compared with men: impact of diabetes mellitus on incremental prognostic value and effect on patient management. *J Am Coll Cardiol.* 2003;41:1125–1133.
18. Germano G, Kiat H, Kavanagh PB, et al. Automatic quantification of ejection fraction from gated myocardial perfusion SPECT. *J Nucl Med.* 1995;36:2138–2147.
19. Slomka PJ, Nishina H, Berman DS, et al. Automatic quantification of myocardial perfusion stress-rest change: a new measure of ischemia. *J Nucl Med.* 2004;45:183–191.
20. Klocke FJ, Baird MG, Lorell BH, et al. ACC/AHA/ASNC Guidelines for the Clinical Use of Cardiac Radionuclide Imaging: Executive Summary—A Report of the American College of Cardiology/American Heart Association Task Force on Practice Guidelines (ACC/AHA/ASNC Committee to Revise the 1995 Guidelines for the Clinical Use of Cardiac Radionuclide Imaging). *Circulation.* 2003;108:1404–1418.
21. Cerqueira MD, Weissman NJ, Dilsizian V, et al. Standardized myocardial segmentation and nomenclature for tomographic imaging of the heart: a statement for healthcare professionals from the Cardiac Imaging Committee of the Council on Clinical Cardiology of the American Heart Association. *Circulation.* 2002;105:539–542.
22. Ladenheim ML, Pollock BH, Rozanski A, et al. Extent and severity of myocardial hypoperfusion as predictors of prognosis in patients with suspected coronary artery disease. *J Am Coll Cardiol.* 1986;7:464–471.
23. Hanley JA, McNeil BJ. The meaning and use of the area under a receiver operating characteristic (ROC) curve. *Radiology.* 1982;143:29–36.
24. Sharir T, Germano G, Waechter PB, et al. A new algorithm for the quantitation of myocardial perfusion SPECT. II. Validation and diagnostic yield. *J Nucl Med.* 2000;41:720–727.
25. Berman DS, Germano G. Interpretation and reporting of gated myocardial perfusion SPECT. In: Germano G, Berman DS, eds. *Clinical Gated Cardiac SPECT.* 2nd ed. Oxford, U.K.: Blackwell Publishing; In press.
26. Choi JY, Lee KH, Kim SJ, et al. Gating provides improved accuracy for differentiating artifacts from true lesions in equivocal fixed defects on technetium 99m tetrofosmin perfusion SPECT. *J Nucl Cardiol.* 1998;5:395–401.
27. DePuey EG, Rozanski A. Using gated technetium-99m-sestamibi SPECT to characterize fixed myocardial defects as infarct or artifact. *J Nucl Med.* 1995;36:952–955.
28. Smanio PE, Watson DD, Segalla DL, et al. Value of gating of technetium-99m sestamibi single-photon emission computed tomographic imaging. *J Am Coll Cardiol.* 1997;30:1687–1692.
29. Wagner A, Mahrholdt H, Holly TA, et al. Contrast-enhanced MRI and routine single photon emission computed tomography (SPECT) perfusion imaging for detection of subendocardial myocardial infarcts: an imaging study. *Lancet.* 2003;361:374–379.
30. Hendel RC, Corbett JR, Cullom SJ, et al. The value and practice of attenuation correction for myocardial perfusion SPECT imaging: a joint position statement from the American Society of Nuclear Cardiology and the Society of Nuclear Medicine. *J Nucl Cardiol.* 2002;9:135–143.
31. Shotwell M, Singh BM, Fortman C, et al. Improved coronary disease detection with quantitative attenuation-corrected Tl-201 images. *J Nucl Cardiol.* 2002;9:52–62.
32. Harel F, Genin R, Daou D, et al. Clinical impact of combination of scatter, attenuation correction, and depth-dependent resolution recovery for ^{201}Tl studies. *J Nucl Med.* 2001;42:1451–1456.